Magnetic Resonance Imaging 59 (2019) 77–87

Contents lists available at ScienceDirect

Magnetic Resonance Imaging

journal homepage: www.elsevier.com/locate/mri

Original contribution

7T CEST MRI: A potential imaging tool for the assessment of tumor grade and cell proliferation in breast cancer

Olgica Zaric[a], Alex Farr[b,*], Esau Poblador Rodriguez[a], Vladimir Mlynarik[a,c], Wolfgang Bogner[a], Stephan Gruber[a], Ella Asseryanis[b], Christian F. Singer[b], Siegfried Trattnig[a,d]

[a] High Field MR Centre, Department of Biomedical Imaging and Image-guided Therapy, Medical University of Vienna, Vienna, Austria
[b] Breast Health Centre, Department of Obstetrics and Gynecology, Medical University of Vienna, Vienna, Austria
[c] Karl Landsteiner Gesellschaft, St. Pölten, Austria
[d] Christian Doppler Laboratory for Clinical Molecular MRI, Christian Doppler Forschungsgesellschaft, Vienna, Austria

ARTICLE INFO

Keywords:
Breast MRI
CEST
Tumor grade
Ki-67 proliferation index

ABSTRACT

Objectives: To investigate the feasibility of chemical exchange saturation transfer (CEST) MRI in patients with breast carcinomas and possible correlations between magnetization transfer asymmetry (MTR_{asym}) values and histological features, such as tumor grade and the Ki-67 proliferation index.

Materials and methods: Nine healthy subjects and 18 female patients were enrolled for this study. The imaging protocol for the patients consisted of diffusion-weighted imaging (DWI), CEST imaging, and T1-weighted, contrast-enhanced (CE)-MRI. CEST was performed using a 3D gradient echo (GRE) sequence, employing eight pre-saturation pulses of a duration of 50 ms and a duty cycle (DC) of 80%, with a mean amplitude of the saturation pulse train of 1 μT. The Z-spectrum was plotted and MTR_{asym} values calculated for the frequency of the maximum of MTR_{asym} curve, were correlated with the Ki-67 proliferation index and apparent diffusion coefficient (ADC). Patient data were statistically assessed using the Games-Howell post-hoc and Pearson's correlation test.

Results: Different tumor types had asymmetry peaks at different positions of Z-spectrum.

MTR_{asym} (mean ± SD) (%) calculated for G1 (3.0 ± 0.3; range: 2.70–3.50) was not significantly lower than for G2 (4.50 ± 1.30; range: 3.20–6.50; $p = 0.066$). In contrast, the increase in MTR_{asym} between G1 and G3 (6.40 ± 1.70; range: 4.80–9.80) lesions was significant ($p = 0.007$). No significant difference was observed between G2 and G3 with regard to MTR_{asym} ($p = 0.089$). There was a strong positive correlation between the MTR_{asym}, and Ki-67 proliferation index ($r = 0.890$; $p = 0.001$), while there was a moderate negative correlation between MTR_{asym} and ADC values ($r = -0.506$; $p = 0.027$).

Conclusions: Calculated MTR_{asym} demonstrates a strong positive correlation with tumor proliferation and has the potential to become a valuable biomarker for breast tumor characterization.

1. Introduction

Magnetic resonance imaging (MRI) for breast lesion detection and characterization, at high fields, is currently based on morphological, contrast-enhanced (CE) MR investigations and diffusion weighted imaging (DWI) [1–3].

In the last two decades, there has been a strong demand for the development and implementation of MR techniques that could not only increase the overall specificity of breast MR examinations, but also provide greater insight into the processes connected with tumorigenesis, growth, and metastasis. Therefore, there is a strong demand for fast alternative proton (1H) MRI techniques that can detect and monitor the concentration changes of different compounds involved in tumor metabolism. One of these techniques is chemical exchange saturation

Abbreviations: ADC, apparent diffusion coefficient; APTw, amide proton transfer weighted; BI-RADS, Breast Imaging Reporting and Data System; B_0, Static magnetic field; B_1, Combined transmit and receive radiofrequency field; $B_{1,sp}$, power of saturation pulses; B_1^+, transmit radiofrequency field; CE, contrast-enhanced; CEST, chemical exchange saturation transfer; DWI, diffusion-weighted imaging; ROI, region-of-interest; RF, radiofrequency field; SAR, specific absorption rate; MTR_{asym}, magnetization transfer ratio asymmetry

* Corresponding author at: Medical University of Vienna, Department of Obstetrics and Gynecology, Breast Health Centre, Waehringer Guertel 18-20, A-1090 Vienna, Austria.
E-mail address: alex.farr@meduniwien.ac.at (A. Farr).

https://doi.org/10.1016/j.mri.2019.03.004
Received 5 February 2019; Received in revised form 3 March 2019; Accepted 4 March 2019

Table 1
Histological characteristics of 18 patients with 19 breast carcinomas and results obtained from contrast-enhanced (CE), diffusion-weighted (DW), and chemical exchange saturation transfer (CEST) magnetic resonance imaging (MRI).

Pat (no)	Age (y)	Size (cm)	Kinetic curve assessment	Histologic type/grade	Phenotype ER/PR/Her2	Ki-67 (%)	ADC × 10^{-3} (mm^2/s)	MTR_{asym} peak (ppm)	MTR_{asym} (%)
1	48	1.8	II	Invasive mucinous Ca/G1	90/80/–	20	0.82	1.20	3.50
2	53	2.0	III	IDC/G2	90/50/–	40	1.11	2.15	4.0
3	54	0.8	I	Papillary in situ/G1	90/90/–	10	1.67	1.45	2.80
4	53	6.0	III	IDC/G3	–/–/90	70	0.91	2.20	5.80
5	60	1.8	II	IDC/G2	80/80/–	20	1.35	1.85	3.20
6	41	4.2	III	IDC/G3	–/–/100	70	0.78	2.0	9.80
7	62	2.5	II	IDC/G3	90/40/–	30	1.27	3.50	5.70
8	49	1.0	II	IDC/G2	90/80/–	50	1.1	1.80	4.20
9	75	0.9	III	ILC/G2	90/90/–	50	0.90	2.30	4.40
10	53	4.5	III	IDC/G3	–/–/–	80	0.81	3.55	4.80
11	71	5.0	II	ILC/G2	40/–/90	20	1.20	1.90	3.30
12	58	1.0	III	IDC/G3	10/–/–	70	0.90	1.95	6.20
12[a]	58	0.8	III	IDC/G3	10/–/–	70	0.90	1.95	6.30
13	62	1.5	III	ILC/G2	90/90/–	60	1.0	3.50	6.0
14	55	0.8	II	IDC/G1	90/80/–	20	1.03	1.25	2.90
15	43	3.5	III	IDC/G2	90/80/–	70	1.02	2.05	6.50
16	64	2.7	III	IDC/G1	90/90/–	20	1.05	1.60	3.10
17	58	1.5	III	IDC/G1	90/10/–	10	1.08	1.30	2.80
18	53	1.3	III	IDC/G1	90/80/–	10	1.0	1.40	2.70

Abbreviations: ADC = apparent diffusion coefficient; DCIS = ductal carcinoma in situ; ER/PR/Her2 = Estrogen/Progesterone/Her2; G1, G2, G3 = grade 1, 2, 3; IDC = invasive ductal carcinoma; ILC = invasive lobular carcinoma; Ki67 = Ki67 proliferation index (%). Kinetic curve assessment: type I-persistent enhancing; type II-plateau; type III-washout; MTR_{asym} = magnetization transfer ratio asymmetry measured at two different spectra positions (1.4 and 2.0 ppm); neg. = negative; ppm = parts per million.

[a] The second lesion in patient #12.

transfer (CEST), which has sparked interest as a novel contrast mechanism in MRI for the molecular investigation of tumors [4–6].

To date, a relatively low number of CEST-MRI applications in breast tumor patients at 3.0 T has been reported [7–9]. Several recent studies have demonstrated a decrease in amide proton transfer weighted (APTw) contrast in breast cancer patients with either a complete or partial chemotherapy response [8,10]. The assessment of lymphatic impairment and interstitial protein accumulation in patients with breast cancer treatment-related lymphedema using APTw was reported as feasible, too [11].

Very few studies on CEST applications in breast tumor characterization have been published to date [7,9]. It is still not clear which CEST contrast is detectable in breast tumors and whether there is any correlation between the CEST frequency range and the histological features of tumors. In a study by Zhang et al. using a lipid-free CEST protocol, an increasing trend of magnetization transfer asymmetry (MTR_{asym}) in estrogen receptor-negative ductal carcinomas was observed, with the largest values at the saturation offset of about 1 ppm. In addition, there was also a strong correlation of MTR_{asym} with the proliferation factor Ki-67 at saturation offsets about 1 ppm and 2 ppm [9].

Considering metabolites involved in tumor metabolism, it is well known that one functional process associated with breast tumors is an increased cell proliferation, which can be detected either by an increase in the choline peak in the MR spectra [12] or by a decrease in apparent diffusion coefficient (ADC) values. ADC is inversely related to tumor cellularity, and is a well-established parameter for breast tumor characterization [13,14]. The cellular marker for proliferation is the Ki-67 protein, which is often used as a verification parameter [15].

As previously mentioned, APTw contrast can have an important role in breast tumor characterization, as well. The findings of two recently published studies [16,17] showed that APTw and glycosaminoglycan (GAG) CEST imaging of healthy breast tissue is, in general, feasible and reproducible at 7 T. Based on this, the initial hypothesis was that either hydroxyl groups from choline or amides from different proteins would be detected in carcinomas. Relating MTR_{asym} with Ki-67 and ADC, we could further estimate whether the increased cell proliferation involved in tumor functioning, may be revealed using CEST MRI. In the present study, we investigated the feasibility of CEST imaging in patients with breast carcinomas at 7 T. Using an MTR_{asym} approach, which can be potentially successfully used in clinical settings, without high spectral resolution and long measurement times, we investigated which metabolite contributes to CEST contrast substantially. It was further explored whether differences in MTR_{asym} in different breast carcinomas are detectable and whether they correlate with tumor grade, the Ki-67 proliferation index, and ADC.

2. Materials and methods

All examinations were approved by the local ethics board and written, informed consent was received from all participants in the study.

2.1. Hardware

MRI was performed on a whole-body 7 T MR scanner with a 70 mT/m gradient amplitude and a 200 mT/m/ms slew rate (Magnetom, Siemens Healthcare, Erlangen, Germany). All participants were measured in the prone position. For ^{1}H-MRI, a dual-tuned (^{1}H/^{31}P), bilateral breast coil (four ^{31}P, four ^{1}H channels; Stark, Erlangen, Germany) was used.

2.2. Healthy volunteers

Nine healthy, female volunteers (mean age, 28.5 years ± 2.0 [standard deviation]; age range: 20–37 years) were enrolled in this study. Four subjects were involved in the sequence optimization (number, duration and power of saturation pulses) and the remaining five volunteers were included in test-retest repeatability measurements. For those measurements, the subjects left the MR scanner between each imaging session.

2.3. Patients and specimens

Eighteen female patients (mean age 56 years ± 9, age range: 41–75 years, median 55 years) (Table 1) who fulfilled the following inclusion criteria were enrolled in this study: age ≥ 18 years; not pregnant; not breastfeeding; suspicious finding on mammography or breast sonogram (classified according to the Breast Imaging Reporting and Data System (BI-RADS 0, 4–5); no previous treatment; and no contraindications for MRI or MRI contrast agents. Patients were selected immediately after conventional diagnostic procedures. Lesions were verified histologically by image-guided, core needle biopsy.

Immunohistochemistry was done on whole tumor tissue sections and evaluated centrally at the Medical University of Vienna by using a standardized protocol, where invasive tumor cells in 20 representative HPF (400 magnification) were visually evaluated and only nuclear staining was scored as positive. The results were documented as the percentage of Ki67-stained nuclei regardless of staining intensity.

2.4. The imaging protocol

We optimized a protocol suitable for the breast cancer investigations and performed a thorough sequence optimization (saturation pulse amplitude, number and duration of pre-saturation pulses), and we tested the repeatability of our CEST imaging protocol on healthy subjects.

In healthy volunteers, the number of pulses, the duration, and the mean amplitude of the saturation pulse train, $B_{1,sp,}$ was optimized using a three-dimensional (3D) gradient echo (GRE) sequence [18] and sampling Z-spectra by 37 offsets (relative to the water Larmor frequency) in the range of ± 4.5 ppm.

Transmit radiofrequency field ($B_1{}^+$) was measured using a two-dimensional (2D) turbo fast low angle shot preceded by a magnetization preparation pulse with the following parameters: echo time, TE = 1.97 ms; repetition time, TR = 6000 ms; bandwidth, BW = 490 Hz/Px; in-plane resolution of 2.5 mm; slice thickness of 10 mm (10 slices); field of view, FoV = 320 mm^2.

The imaging protocol for patients, consisted of a localizer followed by transversal, diffusion-weighted imaging (DWI), CEST imaging, and T1-weighted contrast-enhanced (CE) MRI. The detailed imaging parameters are listed in Table 2.

For the CEST, eight Gaussian pre-saturation pulses of 50 ms duration and a duty cycle (DC) of 80% were employed. A saturation pulse train with the same number of pulses and the mean amplitude of 1μT was used, followed by a segmented gradient echo acquisition with a k-space sampling that used a centric reordering of k-space sampling. Z spectra were plotted by 31 equidistant saturation frequency offsets between −4.0 and +4.0 ppm. A frequency-selective water excitation (with a three-lobe binomial pulse with time-bandwidth product of 10) was used to achieve efficient suppression of unwanted fat signals.

DWI was measured using readout-segmented echo planar imaging (rs-EPI) with two *b*-values (0 and 850 s/mm^2) for maximum contrast-to-noise ratio between normal tissue and malignant tumors [19,20].

Contrast-enhanced MRI (CE-MRI) used the TWIST (time-resolved angiography with stochastic trajectories) sequence [21] (spectral fat saturation; temporal resolution of 14 s). A single dose (0.1 mmol/kg of bodyweight) of the contrast agent (gadoterate meglumine, Dotarem; Guerbet, France) was injected intravenously as a bolus, followed by a 20 mL saline flush after the first of 15 repetitions.

Table 2
Sequence parameters used in this study.

Parameter	CE-MRI	DWI	CEST-MRI
TR/TE [ms]	4.8/2.5	5500/65	85/0.5
FoV [mm^2]	330 × 196	320 × 160	320 × 208
Voxel size [mm^3]	0.7 × 0.7 × 0.7	0.9 × 0.9 × 5	1.7 × 1.7 × 4
Number of slices	176	28	30
Number of averages	10	1	1
Acquisition time [min:sec]	7:43	3:48	13:30

Abbreviations: CE-MRI = contrast-enhanced magnetic resonance imaging; DWI = diffusion-weighted imaging; FoV = field of view; CEST-MRI = chemical exchange saturation transfer magnetic resonance imaging; TR/TE = repetition/echo time.

2.5. Data evaluation and data analysis

2.5.1. Region-of-interest (ROI) selection

Two readers, who were aware that each patient had at least one lesion, prospectively evaluated patient data, in consensus. The readers were not provided with information regarding the histologic subtype. Lesion size was measured on CE images using the largest diameter in one plane. In patients with multi-centric carcinomas, the size was measured so as to select the largest lesion. The readers determined the contrast kinetic parameters of the tumors after contrast medium administration (curve type). Apparent diffusion coefficients (ADC) for the ROIs were calculated.

All CEST-MRI data processing was performed using custom-written scripts in Matlab (Mathworks, Natick, MA, USA). For all data, elastic motion correction was applied with the software provided by the manufacturer (Siemens Corporate Research, Princeton, NJ).

The calculation of the Z-spectra was performed on a pixel-by-pixel basis using spline interpolation of points acquired in experiments with different saturation offsets.

The CEST contrast was quantified by determining MTR_{asym}, as defined by the following expression:

$$MTR_{asym} = \frac{S_{sat}(-\Delta\omega) - S_{sat}(+\Delta\omega)}{S_0} \quad (1)$$

where $S_{sat}(+\Delta\omega)$ and $S_{sat}(-\Delta\omega)$ are the signal intensities obtained by saturating at the frequency of Δω downfield and upfield from the water proton resonance frequency, respectively.

For the B_0 inhomogeneity correction, spectral shifting of the Z-spectra used a smoothing-spline-based correction method [22]. MTR_{asym} values were calculated for two independent scans (scan I and scan II).

In healthy subjects, ROIs were placed in the glandular tissue (mean ROI area, 72 ± 12 mm^2; range: 7–138 mm^2). In patients, for CEST evaluations, ROIs were placed in viable parts of tumors, as demonstrated by high post-contrast signal on T1w images and low ADC values at ADC maps (high contrast uptake and high cellularity are typically used as certain signs of malignancy). ROIs (mean ROI area, 62 ± 19 mm^2; range: 8–112 mm^2) analysis was performed using OSIRIX (Osirix Foundation, Geneva, Switzerland). For all tumors, the position of the maximum MTR_{asym} curve and the MTR_{asym} value at this maximum were evaluated. For healthy volunteers, these two parameters were determined retrospectively, after patient analysis.

2.6. Statistical analysis

Statistical analysis was performed using SPSS statistical software, version 21.0 (SPSS, Chicago, IL). For the repeatability measurements, an interclass correlation coefficient (ICC) (CI = 95%) was used. The MTR_{asym} values measured in different tissue types (tumor G1, G2, G3, and healthy tissue) were assessed via univariate analysis of variance and post-hoc tests (Games-Howell). A p-value ≤0.05 was considered significant. In order to achieve the homogenous patient group, we provided the same calculation with two histologically special carcinomas (invasive mucinous and papillary carcinoma in situ) excluded. For the patient population, the MTR_{asym} values were correlated with the Ki-67 proliferation index (%) and the ADC, also using correlation coefficients statistics.

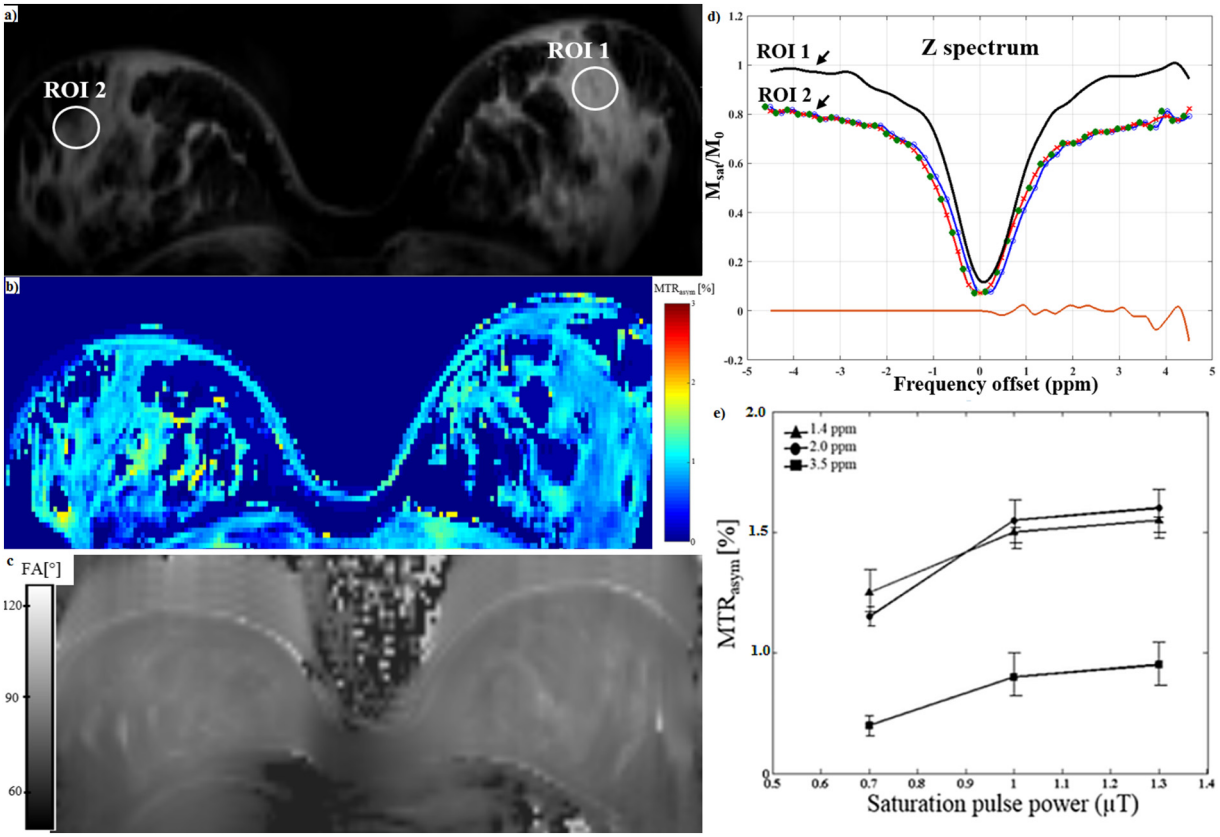

Fig. 1. A CEST experiment performed in a 27-year-old healthy subject.
a) Bilateral axial gradient echo (GRE) image of the breasts without CEST saturation.
b) CEST map calculated for the maximum of MTR_{asym} of 1.4 ppm. The CEST map shows a good agreement in structure delineations (glandular and adipose tissue) with morphological images. It can be seen that value of CEST effect is approximately 0% in adipose tissue.
c) Transmit (B_1^+) RF field map calculated for right and left coil elements. Map shows a relatively good field homogeneity, with up to ± 15% flip angle (FA) variations between different coil parts.
d) Corresponding Z-spectra calculated for two regions-of-interest (ROI 1 and ROI 2, white circles placed in dominantly glandular and mixed glandular-adipose tissue, respectively) show no residual dip at −3.5 ppm that could originate from unsuppressed fat. The Z-spectrum derived for ROI 2 demonstrates all post-processing steps included for an external field (B_0) inhomogeneity correction. The blue dashed line represents nonparametric fitted curve of Z-values, with a smoothing parameter of 0.9; blue line shows measured interpolated data: piecewise cubic hermite polynomial interpolated curve of the measured samples; green line shows shifted interpolated curve according to the calculated water shift; red line shows piecewise cubic hermite polynomial interpolated curve of the corrected samples; red circles show measured samples: Z-values as a function of RF irradiation frequency; green circles represent shifted samples according to the calculated water shift; red cross represents corrected samples: Z-values of the shifted interpolated curve at the RF irradiation frequencies applied; orange line is the asymmetry curve: magnetic transfer ratio asymmetry as the subtraction of negative and positive sides of the B_0 corrected curve.
e) MTR_{asym} calculated for three mean saturation amplitudes of the whole saturation pulse train, $B_{1,sat}$ = 0.7; 1.0; and 1.3 μT, and for three different positions of MTR_{asym} (1.4 ppm, 2.0 ppm, and 3.5 ppm). $B_{1,sat}$ values were chosen in according to the protocol optimization and literature data, while offset frequencies were determined after initial patient measurements. It was necessary to know whether there was any substantial CEST effect that originated from healthy glandular tissue, and whether it contributed to the effect measured in tumor tissue. It can be seen that the highest MTR_{asym} values are for 1.3 μT; however, due to high specific absorption rates (SAR), we used in our experiments pulse power of 1.0 μT. (For interpretation of the references to colour in this figure legend, the reader is referred to the web version of this article.)

3. Results

3.1. Healthy volunteers

MTR_{asym} maps showed a good gland-adipose tissue differentiation (Fig. 1a–b). MTR_{asym} values showed good repeatability of the measurements, at three different chemical shifts: 1.4 ppm, 2.0 ppm and 3.5 ppm, with an ICC of 0.859, 0.914, and 0.756, respectively (Table 3). Results on a protocol optimization are summarized in Table 4.

The average flip angle (FA) values (°) for both coil elements were as follows: for the medial side, 89 ± 8 and, for the lateral side, 75 ± 10. For the prepectoral and retromamillary regions, FA were: 85 ± 7 and 88 ± 5, respectively (Fig. 1c). Z-spectra obtained from mixed glandular-adipose showed no residual dip at −3.5 ppm (Fig. 1d).

The mean MTR_{asym} calculated at 1.4 ppm was 1.25 ± 0.12,

Table 3
Magnetic transfer ratio asymmetries (MTR_{asym}) (mean ± SD) measured in healthy volunteers after B_0 inhomogeneity correction before and after repositioning.

Frequency shift (ppm)	Measurement no.	MTR_{asym} (%)	
1.4	I	1.46 ± 0.40	
	II	1.38 ± 0.30	ICC = 0.859
2.0	I	1.28 ± 0.40	
	II	1.74 ± 0.30	ICC = 0.914
3.5	I	0.75 ± 0.40	
	II	0.69 ± 0.30	ICC = 0.756

Abbreviations: ppm = parts per million; I, II = the first and the second measurement; ICC = interclass correlation coefficient.

Table 4
Magnetic transfer ratio asymmetries (MTR_{asym}) (mean ± SD) measured in healthy volunteers during protocol optimization. The MTR_{asym} values are calculated for set of different saturation pulse powers, $B_{1,sp}$ and duty cycles.

$B_{1,sp}$ (μT)	MTR_{asym}(%) ± SD			
	DC = 20%	DC = 40%	DC = 60%	DC = 80%
0.7	0.80 ± 0.05	1.08 ± 0.06	1.18 ± 0.08	1.25 ± 0.10
1.0	1.00 ± 0.10	1.25 ± 0.09	1.45 ± 0.05	1.55 ± 0.07
1.3	1.30 ± 0.10	1.50 ± 0.10	1.60 ± 0.10	1.68 ± 0.06

Abbreviations: $B_{1,sp}$ = saturation pulse power; DC = duty cycle.

1.55 ± 0.15, and 1.68 ± 0.22 for $B_{1,sp}$ = 0.7 μT, 1.0 μT, and 1.3 μT, respectively (Fig. 1e).

3.2. Patients

In this study, 19 breast lesions were identified (14 invasive ductal carcinoma [IDC], three invasive lobular carcinoma [ILC], one invasive mucinous carcinoma, and one papillary carcinoma in situ). The size of the lesions was 2.3 ± 1.5 cm; range: 0.8–6.0 cm. Fifteen lesions were classified as mass-enhancing and four as non-mass-enhancing lesions (Table 1).

An evaluation of contrast enhanced (CE) images and kinetic curves showed that 18 of 19 lesions had an initial enhancement (the first 90 s) higher than 90%. The mean ADC value for all lesions was 1.10 ± 0.24, range: 0.78–1.67 × 10^{-3} mm^2/s.

The Z-spectrum was plotted for each patient, and the position of the asymmetry dip was determined. This analysis showed that there are three different offsets around which all tumors are grouped: 1.4; 2.0; and 3.5 ppm. In the case of more than one dip detected, the one with the higher MTR_{asym} value was taken. The dependence of frequency offset on tumor grade is shown in Fig. 2a.

In healthy contralateral glandular tissue, the MTR_{asym} value was 1.20 ± 0.40 (range: 0.88–1.33), 1.42 ± 0.80 (range: 0.84–1.52), and 0.72 ± 0.40 (range: 0.55–1.23) at 1.4 ppm, 2.0 ppm, and 3.5 ppm, respectively.

For each carcinoma, the calculated maximum MTR_{asym} values, with the corresponding saturation frequencies are summarized in Table 1. With regard to the grade of tumor differentiation, all G1 lesions (6/6) had the maximum MTR_{asym} at the frequency of 1.4 ppm. For six of the G2 lesions (6/7) and four G3 lesions (4/6), MTR_{asym} maximums were at 2.0 ppm. The remaining one G2 (1/7) and two G3 lesions (2/6) had a higher MTR_{asym} value at 3.5 ppm rather than at 2.0 ppm (Fig. 2b).

MTR_{asym} measured for G1 was 3.0 ± 0.3 (range: 2.70–3.50) and was not significantly lower than that for G2 (4.50 ± 1.30; range: 3.20–6.50; p = 0.066). When G1 and G3 lesions were compared (6.40 ± 1.70; range: 4.80–9.80), there was a significant difference in MTR_{asym} (p = 0.007), but there was no significant difference in MTR_{asym} between G2 and G3 (p = 0.089). When two special types of G1 carcinomas were excluded from the patient group, the mean MTR_{asym} was 2.90 ± 0.20 (range: 2.70–3.10) with p = 0.070 and p = 0.006 compared to G2 and G3 carcinomas, respectively. The MTR_{asym} values measured in the healthy tissue were significantly lower than those in the tumor tissue of each of the tumor grades G1, G2, and G3 (all p ≤ 0.001) (Fig. 2b). The MTR_{asym} maps of patients with G3 and G1 carcinomas are shown in Figs. 3a–d and 4a–d, respectively. Fig. 5a–f, provides an example of a patient with the maximum MTR_{asym} value at 3.5 ppm.

There was a strong positive correlation between the MTR_{asym} value and the Ki-67 proliferation index (r = 0.890; p = 0.001) (Fig. 6a), whereas there was a moderate negative correlation between MTR_{asym} and ADC values (r = −0.506; p = 0.027) (Fig. 6b).

4. Discussion

CEST-MRI at 7 T is a noninvasive, repeatable, and clinically feasible imaging technique that may be used for breast carcinoma characterization.

This study showed that the asymmetry peaks were detected at different positions of the Z-spectrum for different tumor grades. Besides, significant differences in MTR_{asym} values, between low and high tumor grade (G1 and G3), were observed. However, no significant differences in MTR_{asym}, between intermediate grade G2 and G1 and G3 breast carcinomas, were found.

The imaging protocol we used was optimized on healthy volunteers. Data were acquired in the range from −4.5 to +4.5 ppm, and with a 0.28 ppm step size to ensure a broad Z-spectrum coverage of the main metabolite resonance frequencies.

Compared to the protocol of Schmitt et al. [7], we were able to substantially boost the Z-spectral resolution by using 31 saturation offset points in the same frequency range and at the same spatial resolution at 7 T. The duration of our entire protocol for the patients,

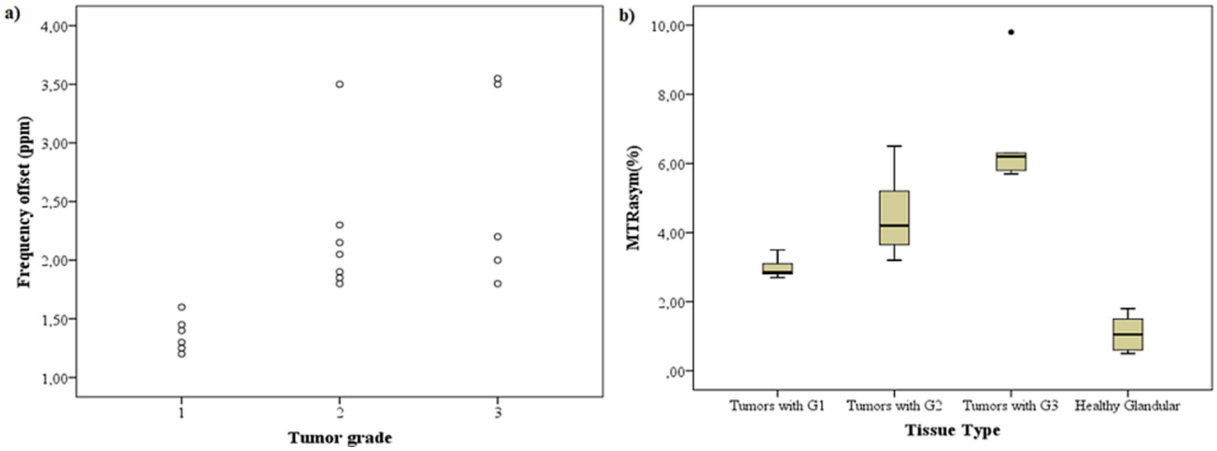

Fig. 2. For each patient the Z-spectrum was plotted, and the position of the asymmetry dip was determined. In the case of more than one dip detected, the one with the higher MTR_{asym} value was taken. a) Diagram shows offset frequency of MTR_{asym} versus tumor grade; it can be noted that there are three different offsets around which tumors are grouped: 1.4; 2.0; and 3.5 ppm. These values were later used for MTR_{asym} map calculations; b) boxplot diagram shows maximal values of MTR_{asym} for healthy glandular tissue from the contralateral side and the same parameter found in carcinomas, which were divided into three groups based on grade 1, 2, and 3 (G1, G2, and G3). Statistical analysis showed significantly higher MTR_{asym} values in tumors (G1, G2, and G3) at 1.4 ppm compared to normal tissue (p = 0.001 in all three cases), respectively.

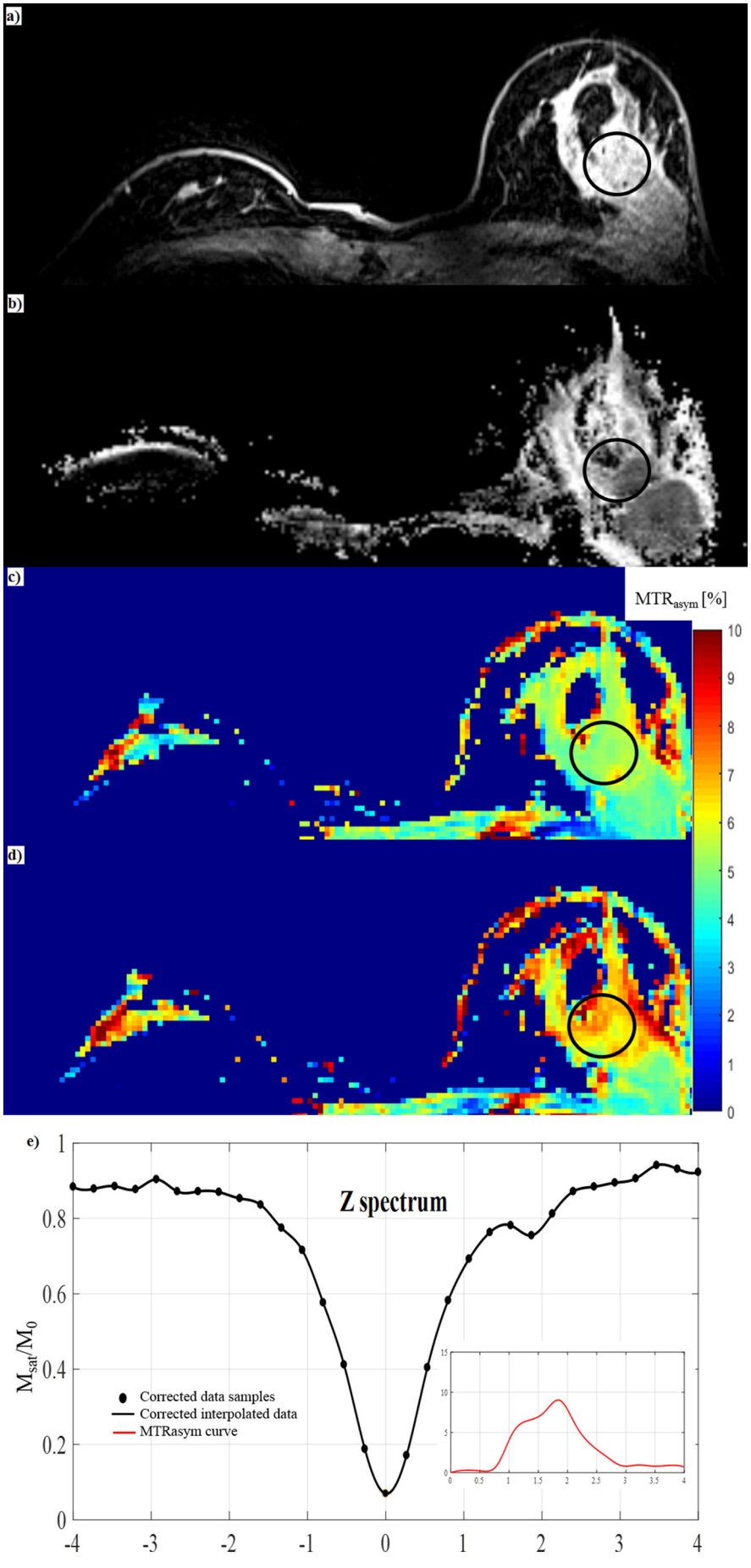

Fig. 3. A 41-year-old female patient with grade 3 (G3) invasive ductal carcinoma in the left breast.
a) Contrast enhancement (CE) imaging showed high initial contrast uptake in the tumor, with irregular margins and no enhancement in a round-shaped lesion histologically described as a fibrotic mass.
b) Apparent diffusion map (ADC) showed a regional decrease in ADC values (regions of high cellularity).
c) CEST map calculated at 1.4 ppm showed lower MTR_{asym} values within the selected region of interest, ROI (black circle) compared to d).
d) CEST map demonstrates shifting the maximum MTR_{asym} curve to higher offsets and a higher CEST effect at 2.0 ppm. Regional changes of the CEST effect can be seen. The area of the tumor with strong contrast uptake corresponds to low ADC values and high CEST effect. Fibrotic mass shows low CEST values at both offset frequencies (1.4 and 2.0 ppm), while the ADC map shows low ADC values. In this case, MTR_{asym} and ADC can indicate that different functional properties of breast tumors may be involved in the formation of CEST contrast.
e) Z-spectra obtained after external field inhomogeneity (B_0) correction from a selected ROI placed at the vital part of tumor shows a dip around 2.0 ppm.

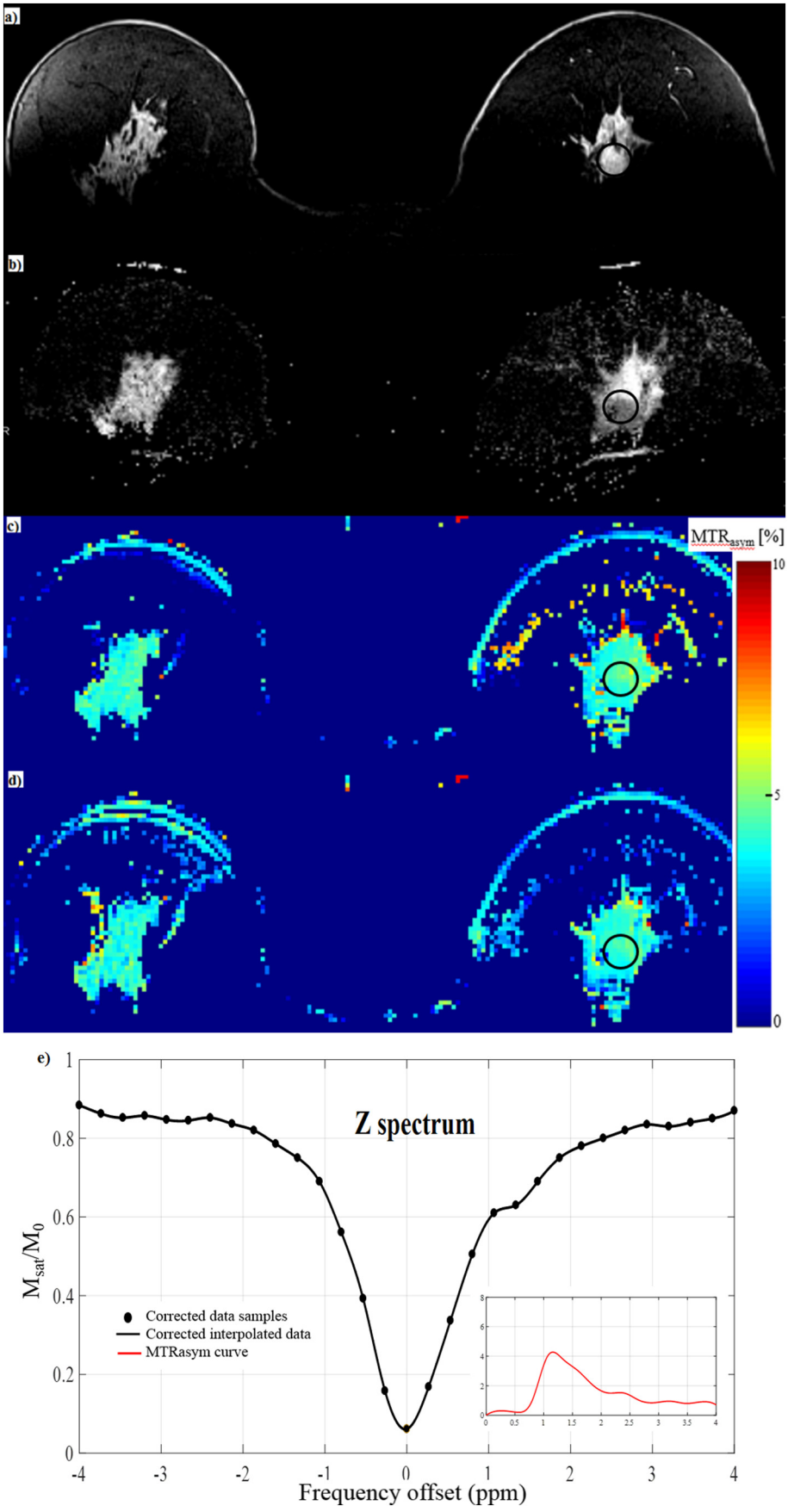

Fig. 4. A 64-year-old female patient with invasive ductal carcinoma of grade 1 (G1) in the left breast.
a) This mass lesion with spiculated margins showed high initial contrast uptake with a relatively homogeneous signal on post-contrast (CE) images.
b) Lower ADC values were measured in the tumor region compared to those in the glandular tissue.
c) CEST map calculated at 1.4 ppm showed slightly higher MTR_{asym} values in the region of interest (ROI (black circle)) of the lesion compared to the contralateral breast tissue. The MTR_{asym} values were increased within the region of high vascularity (high signal on CE images) and high cellularity (low ADC values on ADC map).
d) CEST map calculated at 2.0 ppm, which showed lower MTR_{asym} values compared to those in c). This indicates that the maximum of the MTR_{asym} lines for low grade tumors can be found at lower saturation offsets. The MTR_{asym} value calculated for this tumor is close to MTR_{asym} measured in healthy tissue from the contralateral breast. It should be noted that for this low-grade tumor, the MTR_{asym} value is relatively low compared to high-grade tumors.
e) Z-spectra obtained after external field inhomogeneity (B_0) correction from ROI showed a dip around 1.4 ppm.

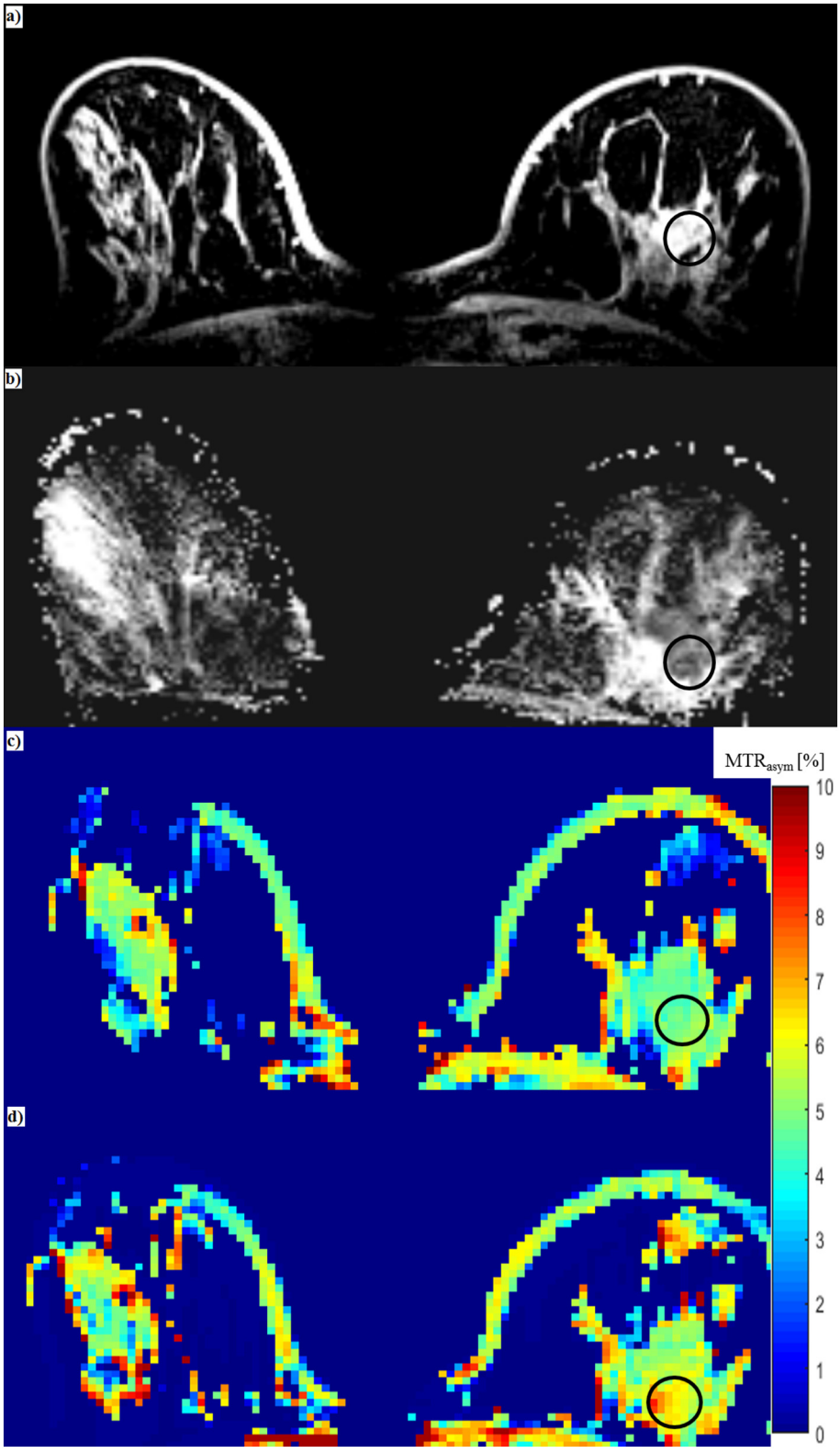

Fig. 5. A 53-year-old female patient with triple-negative grade 3 (G3) invasive ductal carcinoma in the left breast.
a) Post contrast T1w image showed heterogeneous enhancement stronger near the borders of the tumor.
b) ADC maps showed high cellularity (low ADC values) within selected region-of -interest (ROI) (black circle).
c) The CEST map calculated at 1.4 ppm showed very low MTR_{asym} values obtained from the selected ROI.
d) This highly heterogeneous tumor is an example of the existence of two asymmetry peaks at different spectral positions of the Z-spectrum. Figure shows CEST map calculated for the offset frequency of 3.5 ppm. The area of the tumor with a high CEST effect corresponded to low ADC values on the ADC map.
e) After the correction for external field (B_0) inhomogeneity, Z-spectra obtained from ROI demonstrates two dips: the first close to 2.0 ppm and the second, more prominent one at 3.5 ppm.

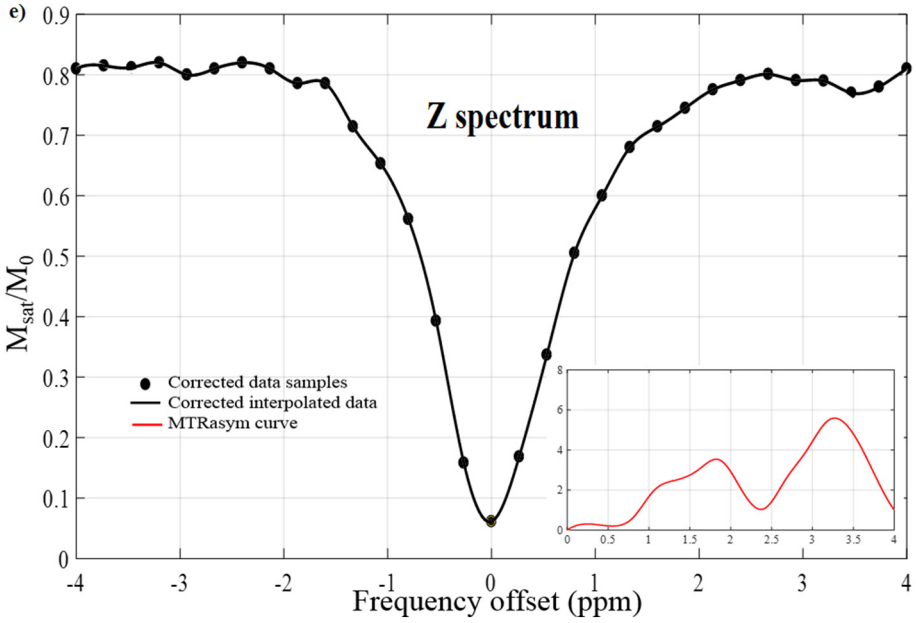

Fig. 5. (*continued*)

including CE-MRI and DWI, was approximately 35 min, which may be feasible in clinical settings. In-plane spatial resolution of 1.7 mm and 4 mm slice thicknesses provided a good trade-off between SNR and the voxel size for sufficiently precise tissue (glandular-adipose) delineation.

The interpretation of in vivo Z-spectra data can be influenced by several factors, such as B_1^+ and B_0 inhomogeneity [23]. To estimate the homogeneity of the transmit RF field, we performed in vivo experiments which showed a relatively good homogeneity of B_1^+ over the entire coil volume and on both element sides (right and left).

CEST contrast showed slightly higher values at 1.3 μT compared to the effect detected for $B_{1,sp}$ of 1.0 μT. However, due to specific absorption rate (SAR) restrictions at high field and the fact that longer and more frequent saturation is more efficient than the shorter (less frequent) and stronger saturation, we employed pulse powers of 1.0 μT, similar to an earlier CEST quantification technique optimization report [24]. The actual $B_{1,sp}$ values at different spatial locations should deviate from the nominal ones only in the B_1^+ variation range (from ± 8 to ± 12%).

MTR_{asym} depends critically on the knowledge of B_0 in each voxel; therefore, voxel-wise B_0 correction, by shifting the Z-spectrum of each voxel to 0 ppm, was applied [22]. The MTR_{asym} in the healthy fibroglandular tissue was low, up to 2%, measured for two frequency ranges (about 1.4 and 2.0 ppm) and < 1% at 3.5 ppm, which was in agreement with recently published data [9]. Repeatability evaluations and interclass correlation coefficient showed good agreement in MTR_{asym} between two independent sets of measurements.

For the fat suppression, we used the water excitation method which is insensitive to B_1^+ inhomogeneity, in contrast to the frequency-selective fat-suppression method.

Our initial assumption was that APTw or choline CEST contrasts would be found in breast tumors. Even though our measurement protocol was not substantially different from those reported by Dula et al. [17] (shown to be feasible for both hydroxyl groups from GAG, and amide detection), our results could not provide clear evidence that either APTw or choline CEST was clearly distinctive for all patients. Our results showed that the asymmetry peaks were detected at different positions of the Z-spectrum for different tumor grades. The shift of the maximum of the MTR_{asym} curve, with the tumor grade, is an additional information compared with measuring MTR_{asym} in a predefined range. With the advances in data processing, extraction of any parameter of the MTR_{asym} curve (shape, position, area under the curve) can be potentially used in clinical practice, as well.

MTR_{asym} measured in viable parts of malignant tumors showed significantly higher values compared to the contralateral healthy glandular tissue. The viable parts of the tumor were determined using post-contrast T1w images. When comparing our data with the histological properties of tumors, we found that the maximum of the MTR_{asym} curve for all low-grade tumors (G1) was observed in a different spectral region than that in moderate- and high-grade tumors (G2 and G3). The $MTR_{asym,}$ value calculated for the saturation frequency of its maximum, demonstrated a high positive correlation with the Ki-67 proliferation index. Making a patient group more homogeneous and excluding the histologically special types of tumors (invasive mucinous and papillary carcinoma in situ) didn't change substantially final statistical results. The ADC values measured in patients were in good agreement with the data available for malignant breast lesions [20]. Based on our hypothesis, and relating MTR_{asym} with ADC, we could estimate whether the cell proliferation involved in tumor functioning, may be detected using CEST-MRI. A correlation analysis between MTR_{asym} and ADC showed moderate correlation between these two parameters. This can be explained by the fact that processes responsible for changes in ADC values may be independent of the processes that influence changes in MTR_{asym} values.

In the case of breast tumors, there are limited data published about the metabolic activity of breast carcinomas and it was difficult to anticipate which type of exchangeable protons would be detectable [25]. The optimization of the measurement protocol and $B_{1,sp}$ have to be determined for each individual application, which makes breast tumor biomarker identification even more difficult when exchange rate and concentration are unknown.

The CEST peak around 1.4 ppm, which we found in the low-grade breast tumors, may originate from –OH protons, from GAG, and/or from choline. Although there are numerous publications that reveal the involvement of these compounds in tumor metabolism, further studies of the role of different chemical species are necessary. Similarly, the origin of the CEST contrast detected at 2.0 ppm is not clear and may be a weighted sum of signals that originate from many different amine groups [26]. Potential contributions from metabolites responsible for the CEST effect, such as glutamate, glucose, proteins, peptides, and changes in pH and relaxation times, cannot be ruled out, either [27].

In our patient population, the APTw contrast increased in only three patients, compared to the healthy glandular tissue. Two recent studies,

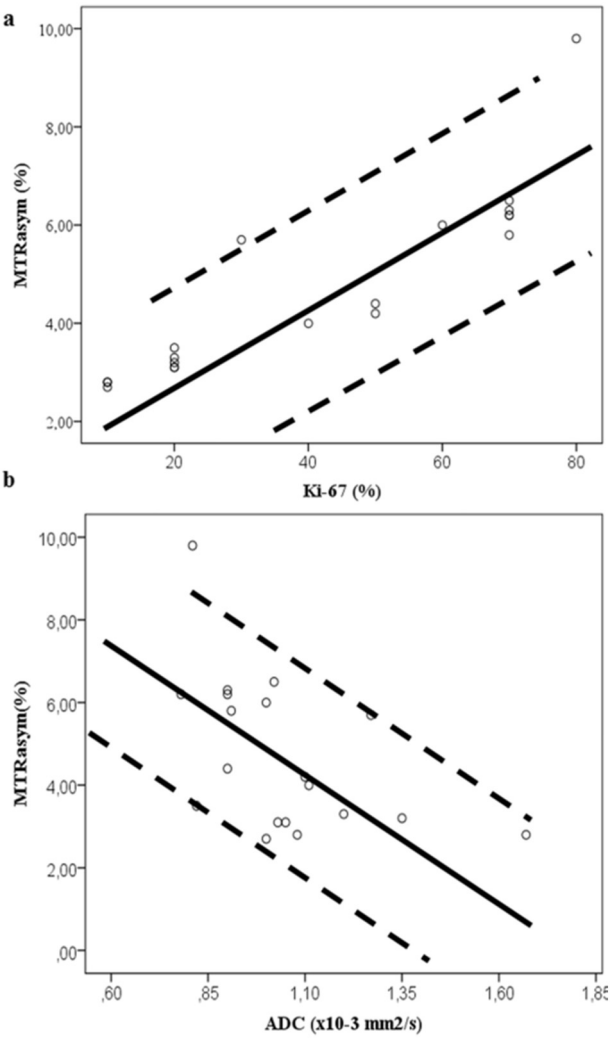

Fig. 6. Graphs show the correlation (solid line) a) between the maximum value of MTR_{asym} (%) and the Ki-67 proliferation index (%) and b) between maximum value of MTR_{asym} and the apparent diffusion coefficient (ADC), measured with a 95% confidence interval (dashed line). Diagrams show a high positive correlation between MTR_{asym} and the Ki-67 proliferation index ($r = 0.890$, $p < 0.001$) and a moderate negative correlation between MTR_{asym} and ADC ($r = -0.506$, $p = 0.027$).

with a limited number of patients, showed that APTw-CEST contrast found in tumors was not statistically different from that in healthy tissue, demonstrating a temporal evolution of APTw-CEST during neoadjuvant chemotherapy [8,10]. Further investigations of a possible relation between APTw-CEST and treatment response are required.

There are several drawbacks of the CEST method. The potential presence of strong lipid signals from the tumor tissue may affect Z-spectra interpretation [28]. When three different tissue types (dominantly glandular and mixed glandular-adipose tissue) were measured, there was no residual dip at −3.5 ppm that could have originated from lipids. However, the situation with fat suppression in breast tumors may be more complicated due to the possible presence of the second and third largest lipid peaks in the Z-spectra, which appear approximately 3.8 ppm upfield and 0.6 ppm downfield from water resonance, respectively [9].

The importance of the suppression of the lipid signal was also demonstrated in a paper by Zhang et al. [9]. They showed that the removal of the lipid signal from the images was useful in detecting the CEST effect in breast tumors, especially in the saturation frequency ranges of 1.8–2.2 ppm and 3.3–3.7 ppm. The reported increase of the MTR_{asym} values in aggressive tumors compared to benign tumors and to normal tissue in all three saturation offset ranges, agrees well with the peak MTR_{asym} values obtained in our study, although direct comparison of the MTR_{asym} magnitudes is difficult due to different data evaluation methodology. Similarly, the reported increase of the MTR_{asym} value with Ki-67 was also observed in our study.

As has been already mentioned, CEST experiments at high fields are associated with technical challenges, such as increased B_0 and B_1 field inhomogeneity [29]. Parallel transmit coils would alleviate this problem [30,31], but have not yet been used for breast MRI. As an alternative to pTX-based B_1^+ inhomogeneity correction, the repeated measurement with two different saturation pulse powers can be used [32], which has, however, the drawback of doubling the scan time.

The general issue with CEST-MRI is low specificity. The MTR_{asym} analysis is the most commonly used and fast method for CEST data analysis; however, it mixes the desirable CEST contrast with direct water saturation (DS), conventional MT contrast (MTC), and nuclear Overhauser enhancement (NOE) components. MTR_{asym} is unable to correct for any MT effects up-field from water, which is observed as a broad asymmetric component of NOE effects in vivo [33]. Therefore, different methods for Z-spectrum analysis that can separate these effects should be considered [34]. Also, future methodological developments that would enable a description of multi-pool CEST contrast may be potentially useful for quantifying in vivo CEST applications [35].

In addition, it is still challenging to remove overlapping CEST signals from different neighboring exchanging sites. The APT signal for example, could be contaminated by CEST effects from fast-exchanging amines at 3.0 ppm and intermediate-exchanging amines at 2.0 ppm. The development of exchange-dependent relaxation rate (Rex) methods may overcome this limitation [36].

In breast cancer patients, CEST contrast may be influenced by T1 relaxation time [37]. Due to prolonged scan times and clinical impracticability, we did not correct for different T1 values in tumors, but we did ensure that dynamic CE-MRI was performed after the CEST measurement to avoid bias due to the associated dynamic T1 changes.

Small number of patient is a limitation of this study. Even though that we showed that excluding the histologically special cases does not substantially affect the results, we believe that larger and heterogeneous patient population confirming our findings should be studied in the future. This could further enhance the potential clinical application of the CEST technique.

Relatively low resolution used in this study, could not provide analysis of the tumor borders with the high accuracy. Therefore, we selected the circle ROIs including the vital and, excluding (even though very small) necrotic parts of tumors. Thus, detection of other metabolites, involved the breast cancer metabolism, was limited. Breast MR examinations are usually performed with the subject in the prone position to reduce the negative effects of breathing. However, it is critically important to choose effective retrospective compensation for motion using non-rigid registration techniques or to choose motion-insensitive acquisition strategies. In this study, we used an elastic registration algorithm and a relatively large voxel volume to prevent the errors in the asymmetry calculations that can be induced by breathing.

5. Conclusion

CEST-MRI of the breast may potentially provide complementary information on histological features of breast tumors. The CEST signal from healthy glandular tissue differs from malignant tissue as well as between different tumor types. Future technical improvement of this technique, in terms of specificity increase, is necessary. With biochemical and clinical validation, CEST-MRI shows the potential to become another useful and non-invasive biomarker for breast tumor diagnosis and characterization.

Acknowledgements

The authors would like to thank Claudia Kronnerwetter (MRI Technologist) for performing patient examinations. We are also grateful to Dr. Benjamin Schmitt, who provided the MR sequence used in the study.

Funding

This study was funded by the Vienna Science and Technology Fund (WWTF; Project LS14-096) and the OeNB Jubilaeumsfond (grant 16133).

References

[1] Menezes, G.L., et al., Magnetic resonance imaging in breast cancer: a literature review and future perspectives. World J Clin Oncol, 2014. 5(2): p. 61–70.
[2] Pinker, K., et al., Clinical application of bilateral high temporal and spatial resolution dynamic contrast-enhanced magnetic resonance imaging of the breast at 7 T. Eur Radiol, 2014. 24(4): p. 913–20.
[3] Marino, M.A., et al., Multiparametric MRI of the breast: a review. J Magn Reson Imaging, 2018. 47(2): p. 301–315.
[4] Ward KM, Aletras AH, Balaban RS. A new class of contrast agents for MRI based on proton chemical exchange dependent saturation transfer (CEST). J Magn Reson 2000;143(1):79–87.
[5] Vinogradov E, Sherry AD, Lenkinski RE. CEST: from basic principles to applications, challenges and opportunities. J Magn Reson 2013;229:155–72.
[6] van Zijl PC, Yadav NN. Chemical exchange saturation transfer (CEST): what is in a name and what isn't? Magn Reson Med 2011;65(4):927–48.
[7] Schmitt, B., et al., A new contrast in MR mammography by means of chemical exchange saturation transfer (CEST) imaging at 3 Tesla: preliminary results. Rofo, 2011. 183(11): p. 1030–6.
[8] Dula, A.N., et al., Amide proton transfer imaging of the breast at 3 T: establishing reproducibility and possible feasibility assessing chemotherapy response. Magn Reson Med, 2013. 70(1): p. 216–24.
[9] Zhang, S., et al., CEST-Dixon for human breast lesion characterization at 3 T: a preliminary study. Magn Reson Med, 2018.
[10] Krikken E, et al. Amide chemical exchange saturation transfer at 7 T: a possible biomarker for detecting early response to neoadjuvant chemotherapy in breast cancer patients. Breast Cancer Res 2018;20(1):51.
[11] Donahue, M.J., et al., Assessment of lymphatic impairment and interstitial protein accumulation in patients with breast cancer treatment-related lymphedema using CEST MRI. Magn Reson Med, 2016. 75(1): p. 345–55.
[12] Bolan PJ, et al. Imaging in breast cancer: magnetic resonance spectroscopy. Breast Cancer Res 2005;7(4):149–52.
[13] Hatakenaka, M., et al., Apparent diffusion coefficients of breast tumors: clinical application. Magn Reson Med Sci, 2008. 7(1): p. 23–9.
[14] Gruber, S., et al., Diffusion-weighted imaging of breast tumours at 3 Tesla and 7 Tesla: a comparison. Eur Radiol, 2016. 26(5): p. 1466–73.
[15] Yoshikawa, M.I., et al., Relation between cancer cellularity and apparent diffusion coefficient values using diffusion-weighted magnetic resonance imaging in breast cancer. Radiat Med, 2008. 26(4): p. 222–6.
[16] Klomp, D.W., et al., Amide proton transfer imaging of the human breast at 7T: development and reproducibility. NMR Biomed, 2013. 26(10): p. 1271–7.
[17] Dula, A.N., et al., Optimization of 7-T chemical exchange saturation transfer parameters for validation of glycosaminoglycan and amide proton transfer of fibroglandular breast tissue. Radiology, 2015. 275(1): p. 255–61.
[18] Schmitt, B., et al., Optimization of pulse train presaturation for CEST imaging in clinical scanners. Magn Reson Med, 2011. 65(6): p. 1620–9.
[19] Bogner, W., et al., Diffusion-weighted MR for differentiation of breast lesions at 3.0 T: how does selection of diffusion protocols affect diagnosis? Radiology, 2009. 253(2): p. 341–51.
[20] Bogner, W., et al., Bilateral diffusion-weighted MR imaging of breast tumors with submillimeter resolution using readout-segmented echo-planar imaging at 7 T. Radiology, 2015. 274(1): p. 74–84.
[21] Le, Y., et al., Development and evaluation of TWIST Dixon for dynamic contrast-enhanced (DCE) MRI with improved acquisition efficiency and fat suppression. J Magn Reson Imaging, 2012. 36(2): p. 483–91.
[22] Stancanello, J., et al., Development and validation of a smoothing-splines-based correction method for improving the analysis of CEST-MR images. Contrast Media Mol Imaging, 2008. 3(4): p. 136–49.
[23] Liu, G., et al., Nuts and bolts of chemical exchange saturation transfer MRI. NMR Biomed, 2013. 26(7): p. 810–28.
[24] Kim, J., et al., A review of optimization and quantification techniques for chemical exchange saturation transfer MRI toward sensitive in vivo imaging. Contrast Media Mol Imaging, 2015. 10(3): p. 163–178.
[25] Chan, K.W., et al., CEST-MRI detects metabolite levels altered by breast cancer cell aggressiveness and chemotherapy response. NMR Biomed, 2016. 29(6): p. 806–16.
[26] Jin, T., et al., Magnetic resonance imaging of the Amine-Proton EXchange (APEX) dependent contrast. Neuroimage, 2012. 59(2): p. 1218–27.
[27] Cai, K., et al., Creatine CEST MRI for differentiating gliomas with different degrees of aggressiveness. Mol Imaging Biol, 2017. 19(2): p. 225–232.
[28] Shmueli, K., et al., Investigating lipids as a source of chemical exchange-induced MRI frequency shifts. NMR Biomed, 2017. 30(4).
[29] Trattnig S, et al. Key clinical benefits of neuroimaging at 7T. Neuroimage 2018;168:477–89.
[30] Tse DH, et al. Tse DH, et al. B1 + inhomogeneity mitigation in CEST using parallel transmission. Magn Reson Med 2017;78(6):2216–25.
[31] Kim, J., et al., Development of a 7 T RF coil system for breast imaging. NMR Biomed, 2017. 30(1).
[32] Windschuh, J., et al., Correction of B1-inhomogeneities for relaxation-compensated CEST imaging at 7 T. NMR Biomed, 2015. 28(5): p. 529–37.
[33] Hua, J., et al., Quantitative description of the asymmetry in magnetization transfer effects around the water resonance in the human brain. Magn Reson Med, 2007. 58(4): p. 786–93.
[34] Zaiss M, Schmitt B, Bachert P. Quantitative separation of CEST effect from magnetization transfer and spillover effects by Lorentzian-line-fit analysis of z-spectra. J Magn Reson 2011;211(2):149–55.
[35] Sun PZ. Simplified and scalable numerical solution for describing multi-pool chemical exchange saturation transfer (CEST) MRI contrast. J Magn Reson 2010;205(2):235–41.
[36] Zhang, X.Y., et al., Increased CEST specificity for amide and fast-exchanging amine protons using exchange-dependent relaxation rate. NMR Biomed, 2018. 31(2).
[37] Stanisz, G.J., et al., T1, T2 relaxation and magnetization transfer in tissue at 3T. Magn Reson Med, 2005. 54(3): p. 507–12.